IEEE Photonics Journal
An IEEE Photonics Society Publication

Open Access

An Electrically Tunable Polarizer for a Fiber System Based on a Polarization-Dependent Beam Size Derived From a Liquid Crystal Lens

Volume 6, Number 3, June 2014

Michael Chen
Chyong-Hua Chen
Yinchieh Lai
Yan-qing Lu
Yi-Hsin Lin

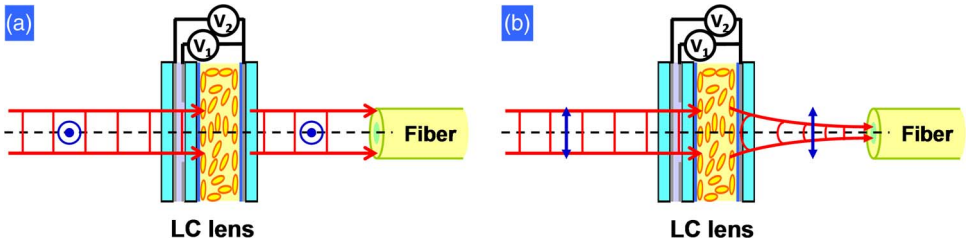

DOI: 10.1109/JPHOT.2014.2319103
1943-0655

IEEE photonics SOCIETY

IEEE

An Electrically Tunable Polarizer for a Fiber System Based on a Polarization-Dependent Beam Size Derived From a Liquid Crystal Lens

Michael Chen,[1] Chyong-Hua Chen,[1] Yinchieh Lai,[1] Yan-qing Lu,[2] and Yi-Hsin Lin[1]

[1]Department of Photonics, National Chiao Tung University, Hsinchu 30010, Taiwan
[2]Department of Materials Science and Engineering and National Laboratory of Solid State Microstructures, Nanjing University, Nanjing 210093, China

DOI: 10.1109/JPHOT.2014.2319103

Manuscript received April 4, 2014; accepted April 16, 2014. Date of publication April 24, 2014; date of current version May 5, 2014. This work was supported by theTaiwanese National Science Council (NSC) under Contract 101-2112-M-009-011-MY3 and Contract 102-2221-E-009-152-MY3. Corresponding author: C.-H. Chen (e-mail: chyong@mail.nctu.edu.tw).

Abstract: A broadband electrically tunable variable polarizer for fiber systems based on a liquid crystal lens is proposed and demonstrated. The polarization selectivity is based on a polarization-sensitive coupling efficiency to the fiber in the fiber system. For an incident ordinary ray, the output beam size remains the same as that of the incident beam, which results in low coupling efficiency. For an incident extraordinary ray (e-ray), the output beam size is close to the size of the fiber core, giving rise to high coupling efficiency because of the lens effect. Moreover, the output beam size of the e-ray can be electrically controlled, thus allowing the optical attenuation to be manipulated. In our experiments, the polarization-dependent loss from the visible to the near-infrared spectral region was approximately 12 dB. Such a broadband electrically variable polarizer may be applied to various designs for fiber-optic sensing devices and polarization-sensitive optical instruments.

Index Terms: Fiber-optic systems, liquid crystal lens, polarizers.

1. Introduction

In addition to the well-known flat panel display (FPD) technology, liquid crystal (LC) technology also plays an important role in various photonic applications, from the visible to the infrared band and even to the terahertz band. Unlike FPD devices, in which the modulation of the light intensity is the primary consideration, the polarization, phase and wavefront of the light are also key factors that should be taken into account in many photonic applications. Because of the electric-field-induced variable birefringence of LCs, many types of light manipulation, including polarization control, light diffraction, and the lens effect, can be achieved through LC phase modulation [1]. Photonic applications offer novel opportunities for the next-generation LC industry, with a much wider spectral range and considerably greater freedom from the optics point of view. To date, many interesting LC devices have been proposed, demonstrated and even commercialized, such as adaptive lenses [2]–[4], bio-sensors [5]–[7], variable optical attenuators [8], [9], optical vortex generators [10], [11], and fiber-optic in-line polarizers [12]. Recently, many wideband in-fiber

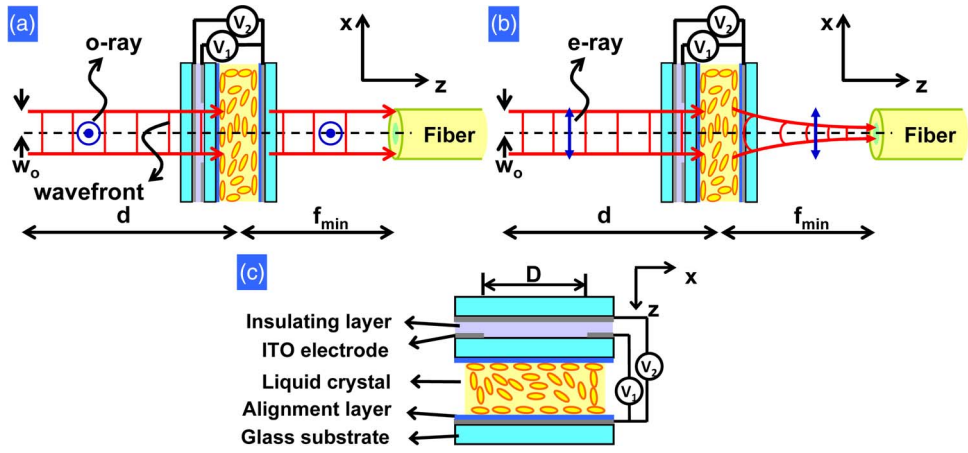

Fig. 1. Schematic diagrams of the operation of an electrically variable polarizer based on the polarization-dependent beam size produced using a LC lens (a) for o-ray incidence and (b) for e-ray incidence. (c) The detailed structure of the LC lens represented in Figs. 1(a) and (b).

polarizers have been proposed because of emerging technologies for fiber-based broadband light sources, e.g., superluminescent LED lights and supercontinuum lasers [13], [14]. However, the polarization-dependent loss (PDL) of such devices strongly depends on the operating wavelength because of the accompanying restrictions on material properties and device structures. These restrictions constitute the primary reason why the PDL remains below 10 dB for the short-wavelength range, which limits the applications of these devices in the visible region [13], [14]. In addition, there is a current trend toward implementing optoelectronic devices with multiple functions for more compact packaging and the inspiration of novel applications. LCs have great potential for multiple-function polarization-sensitive systems because of the versatility of the light-modulation possibilities offered by LCs as a result of their field-sensitive birefringence. In our previous work, we have focused on the development of various electrically tunable LC lenses whose lensing effect originates from a distribution of the spatial orientations of LC molecules under an inhomogeneous electric field [2]–[4], [15], [16]. Many applications, including a pico-projector [17], optical zoom [18], concentrated photovoltaic systems [19], holographic systems [20], endoscopic systems [21], and an ophthalmic lens [22], have been demonstrated. In general, the lens power (i.e., the reciprocal of the focal length) of an LC lens is electrically tunable with high polarization sensitivity. Our objective is to combine the functions of optical-power regulation and polarization selection based on an LC lens for fiber systems. In this paper, we demonstrate a broadband, electrically tunable polarizer based on an LC lens. An arbitrary incident beam entering the nematic LC is split into an extraordinary ray (e-ray) and an ordinary ray (o-ray) whose vibration directions are parallel and perpendicular to the alignment direction of the LC, respectively. As the LC lens has a high lens power for the e-ray, it sees a parabolic phase distribution, giving rise to a convergence of the e-ray with a beam waist that is closely matched to the core radius of the fiber. Therefore, a large amount of the e-ray is directed into the fiber, resulting in a small power loss. By contrast, the o-ray sees a uniform phase distribution, which has no influence on the beam size, and thus experiences a large power loss after propagating through the fiber. The PDL is greater than 12 dB for a broad wavelength range from the visible region to the near-infrared region. In addition, the optical power of the e-ray coupling to the fiber can be controlled by electrically tuning the lens power of the LC lens. We believe that the system proposed in this study has many potential applications in optical fiber sensors, fiber-optic gyroscopes and supercontinuum light systems.

2. Mechanism and Operating Principles

The operating principles of an LC lens for variable polarization selection are schematically illustrated in Fig. 1(a) and (b). Assume the incident wave is a Gaussian beam with a minimum

beam-waist radius of w_o. Let the distance between the multimode fiber and the LC lens be $f_{\min}$ and the lens power of the LC lens be P_{LC}, the reciprocal of the focal length of the LC lens. Because the waist of the incident beam is located at a distance d in front of the lens, the ABCD matrix that represents the transformation of the incident wave in this system is computed as follows:

$$\begin{pmatrix} A & B \\ C & D \end{pmatrix} = \begin{pmatrix} 1 & f_{\min} \\ 0 & 1 \end{pmatrix} \cdot \begin{pmatrix} 1 & 0 \\ -P_{LC} & 1 \end{pmatrix} \cdot \begin{pmatrix} 1 & d \\ 0 & 1 \end{pmatrix}. \tag{1}$$

From the ABCD formulation in Eq. (1), the beam waist (w) at the entrance of the fiber is

$$w = \sqrt{\frac{A^2 + a \cdot B^2}{a \cdot (A \cdot D - B \cdot C)} \cdot \frac{\lambda}{\pi}} \tag{2}$$

where $a = \lambda/(\pi \times w_o^2)$ and λ is the wavelength of the incident light. This formulation can also be rewritten as follows:

$$w = \frac{\sqrt{\pi^2 \cdot w_o^4 \cdot (1 - f_{\min} \cdot P_{LC})^2 + \lambda^2 \cdot [f_{\min} + d \cdot (1 - f_{\min} \cdot P_{LC})]^2}}{\pi \cdot w_o}. \tag{3}$$

The beam waist at the entrance of the fiber can be manipulated by varying P_{LC}. For the o-ray, P_{LC} is always zero because the o-ray experiences a uniform phase distribution in the LC lens. By contrast, for the e-ray, P_{LC} varies because of the variable inhomogeneous phase distribution of the LC lens, which can be manipulated by adjusting the applied voltage. Therefore, the beam waist w of the o-ray is nearly equal to w_o because the propagation distance is short compared to the Rayleigh range, whereas the beam waist of the e-ray is modified.

The coupling coefficient η of the light entering the multimode fiber can be calculated by [23]

$$\eta = \left[1 - \exp\left(-\frac{2 \cdot \rho^2}{M^2 \cdot w^2}\right)\right] \cdot \left[1 - \exp\left(-\frac{2 \cdot NA_{fiber}^2}{M^2 \cdot \theta^2}\right)\right]. \tag{4}$$

where ρ and NA_{fiber} are the core radius and numerical aperture (NA) of the multimode fiber, respectively. θ is the beam divergence of the beam that is incident on the fiber, and M^2 is the beam-propagation factor, which is defined as $M^2 \equiv \pi \times w \times \theta/\lambda$. Equation (4) indicates that the coupling efficiency for the coupling into the multimode fiber is affected not only by the ratio of the incident beam size to the fiber core radius but also by the ratio of NA_{fiber} to θ. In our experiments, the NA of the LC lens (< 0.02) was much smaller than the NA_{fiber} (> 0.1). As a result, Eq. (4) was approximately equal to

$$\eta = \left[1 - \exp\left(-\frac{2 \cdot \rho^2}{M^2 \cdot w^2}\right)\right]. \tag{5}$$

As can be seen from Eqs. (3) and (5), the coupling efficiency for the e-ray can be altered by changing P_{LC}, but the coupling efficiency for the o-ray remains small because of the much larger beam waist w compared to the core size of the fiber. The LC lens behaves as a polarizer because the w of the e-ray is adjusted by the lens power of the LC lens to be close to ρ. Moreover, because the w of the e-ray remains larger than ρ, the attenuation of the e-ray can be continuously controlled.

Next, we introduce the operation of the LC lens illustrated in Fig. 1(c) in greater detail. To demonstrate the concept, we adopt an LC lens with a hole-patterned structure [2], [3], [24]. The LC lens was composed of glass substrates coated with electrodes of indium tin oxide (ITO) layers, a nematic LC MLC-2070 (Merck, $\Delta n = 0.2609$ at 20 °C, 589.3 nm) with a thickness of 50 μm, alignment layers of polyvinyl alcohol (PVA), and an insulating layer (NOA81, Norland Products, Inc.). The alignment layers of PVA were mechanically buffered to align the LC molecules in a certain direction. A hole was etched in the ITO layer on the middle substrate to establish an inhomogeneous electric-field distribution by applying an alternating-current (AC) voltage of V_1. The NOA81 insulating

layer was used to provide separation from the other electrode, to which was applied an AC voltage of V_2. In such a system, when the same voltage is applied to both the homogeneous and the hole-patterned electrodes (i.e., $V_1 = V_2$), the LC molecules are uniformly reoriented, causing P_{LC} for the e-ray to be zero. When $V_1 > V_2$, the LC molecules near the peripheral region of the LC lens are more perpendicular to the glass substrate, and those near the center of the LC lens are more parallel to the glass substrate. As a result, the e-ray travels more slowly through the center of the LC lens than through the peripheral region. The spatial phase distribution thus becomes parabolic, and the LC lens behaves as a positive lens. However, the o-ray encounters a uniform refractive-index distribution regardless of the applied voltage, and P_{LC} remains zero for the o-ray. Because the LC lens is a positive lens, the w of the e-ray is close to ρ, and that of the o-ray is much larger than ρ. Thus, the LC lens functions as a polarizer. As V_2 is gradually increased, while keeping $V_1 > V_2$, the positive P_{LC} for the e-ray decreases, and the output power in the fiber decreases because w is larger than ρ. In this manner, the attenuation of the light transmitted by the fiber can be continuously controlled. For the e-ray, P_{LC} is determined by the difference in refractive index Δn between the center and the edge of the aperture, which can be expressed as [3]

$$P_{LC}(V_1, V_2) = \frac{8 \cdot \Delta n(V_1, V_2) \cdot d_{LC}}{D^2} \tag{6}$$

where D is the aperture size of the tunable lens coupler, and d_{LC} is the thickness of the LC layer. For the o-ray, $P_{LC}(V_1, V_2)$ is zero because $\Delta n(V_1, V_2) = 0$. For the e-ray, P_{LC} can be manipulated by adjusting the applied voltages V_1 and V_2. It is therefore possible to adjust the beam size and coupling efficiency of the e-ray, as shown in Eqs. (3) and (5), whereas the coupling efficiency for the o-ray remains independent of the applied voltages. Therefore, an LC lens combined with an optical fiber can behave as a polarization selector with the capability of variable attenuation. The concept presented here can be applied to other structures of LC lenses. Moreover, it can also be extended to other tunable focusing anisotropic lenses as long as P_{LC} can be electrically switched from positive one to zero.

3. Experiments and Discussions

To investigate the polarization dependency, a wavefront sensor (Thorlabs WFS150-7AR) was used to record the wavefronts after the o-ray and e-ray passed through the LC lens for $(V_1, V_2) = (85\ V_{rms}, 0\ V_{rms})$ at a wavelength λ of 633 nm. The aperture size of the LC lens (D) was 1.33 mm. Fig. 2(a) and (b) present the wavefronts of the o-ray and the e-ray, respectively. No lensing effect was observed because the o-ray experienced a uniform phase distribution in the LC lens. Nevertheless, the LC lens behaved as a positive lens for the e-ray, and the optical path difference (OPD) between the center and the peripheral regions was 6.66 μm. P_{LC} could be calculated using the expression $P_{LC} = 8 \times OPD/D^2$, yielding a value of 30 m^{-1} for P_{LC} in Fig. 2(b). As a result, the e-ray experienced an inhomogeneous phase distribution, resulting in a focused beam. Therefore, this LC lens was confirmed to exhibit a linear polarization selectivity based on the anisotropic lens power. We measured P_{LC} for the e-ray under various applied voltages of the LC lens. We placed the LC lens between two crossed polarizers with a rubbing direction of 45° with respect to the transmission axes of the polarizers and then observed the phase profiles. Fig. 2(c) and (d) present the phase profiles of the LC lens at $(V_1, V_2) = (85\ V_{rms}, 0\ V_{rms})$ and $(85\ V_{rms}, 85\ V_{rms})$. Two adjacent concentric rings represent a phase difference of 2π radians. Assume the number of concentric rings is N; then, $\Delta n \times d_{LC}$ is equal to $N \times \lambda$. According to Eq. (6), P_{LC} then becomes $8 \times N \times \lambda/D^2$. As a result, the voltage dependency of P_{LC} could be calculated from the phase profiles as plotted in Fig. 2(e). The LC lens has a positive P_{LC} as V_2 changes from 0 to 90 V_{rms} for $V_1 = 85\ V_{rms}$. Based on the phase profile at $\lambda = 633$ nm, the calculated P_{LC} then ranges from 0 m^{-1} to 30.3 m^{-1}. To obtain P_{LC} in the infrared region, the dispersion relation for LC materials as described by Cauchy's equation was used [1]. Cauchy's equation is expressed as follows: $n_{o,e} = A_{o,e} + B_{o,e} \cdot \lambda^{-2} + C_{o,e} \cdot \lambda^{-4}$, where n_e and n_o are the refractive indices for the extraordinary and ordinary waves, respectively. The coefficients A_e, B_e, C_e, A_o, B_o, and C_o were

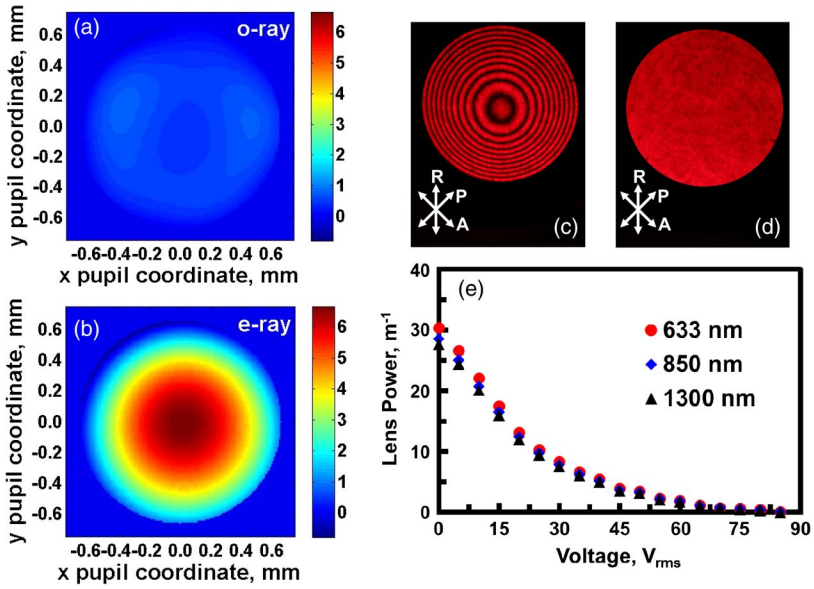

Fig. 2. Wavefronts for (a) the o-ray and (b) the e-ray at $\lambda = 633$ nm. $(V_1, V_2) = (85\ V_{rms}, 0\ V_{rms})$. The color bar indicates the optical path in μm. Phase profiles observed using crossed polarizers at (c) $(V_1, V_2) = (85\ V_{rms}, 0\ V_{rms})$ and (d) $(V_1, V_2) = (85\ V_{rms}, 85\ V_{rms})$. R is the rubbing direction. P and A are the transmission axes of the polarizer and the analyzer, respectively. f = 1 kHz, and $\lambda = 633$ nm. (e) The lens power of the LC lens for the e-ray as a function of the applied voltage V_2 at wavelengths of 633 nm (red dotted curve), 850 nm (blue diamond curve), and 1300 nm (black triangle curve). $V_1 = 85\ V_{rms}$.

measured using an Abbe refractometer. The measured results for MLC-2070 were $A_e = 1.7180$, $B_e = 0.0119\ \mu m^2$, $C_e = 0.0031\ \mu m^4$, $A_o = 1.4899$, $B_o = 0.0095\ \mu m^2$, and $C_o = 0.0002\ \mu m^4$. Using Cauchy's equation for LC materials and the voltage-dependent P_{LC} results at $\lambda = 633$ nm, P_{LC} values for λ of 850 nm and 1300 nm are presented in Fig. 2(e). P_{LC} was found to range from 0 m^{-1} to 28.5 m^{-1} for $\lambda = 850$ nm and from 0 m^{-1} to 27.7 m^{-1} for $\lambda = 1300$ nm. Because of the normal dispersion of the LC materials, the tunable lens-power range decreases as the wavelength increases.

To measure the coupling efficiency, we used three laser light sources (Melles Griot 05-srp-812 for $\lambda = 633$ nm, Power Technology APMT65(850–100)X26 for $\lambda = 850$ nm, and Agilent/HP 81552SM for $\lambda = 1300$ nm). A collimated incident beam with a diameter of 0.8 mm was obtained after the beam produced by each laser source passed through a single-mode fiber (Thorlabs SM600 for the visible range and Thorlabs SMF-28e+ for infrared wavelengths) and a corresponding collimator (Thorlabs F230FC-B for $\lambda = 633$ nm and $\lambda = 850$ nm and Thorlabs F230FC-C for $\lambda = 1300$ nm). The collimated beam passed through a polarizer and then the LC lens. The transmission axis of the polarizer was parallel or perpendicular to the mechanically buffered rubbing direction of the LC layer for the generation of the e-ray or the o-ray, respectively. A multimode fiber with a length of 30 cm (Newport, F-MLD-500, core/cladding diameters of 100 μm/140 μm, NA = 0.29) was placed at a position behind the LC lens that depended on the maximum lens power (i.e., the minimum focal length), as shown in Fig. 2(e). The distance between the multimode fiber and the LC lens was $\sim$3.5 cm. A power meter (OPHIR AN/2 for the visible range and Newport 1916-R for the infrared range) was used to measure the powers before and after the multimode fiber. The fiber was sufficiently short that the absorption in the fiber is neglected. Hence, the ratio of the power after the multimode fiber to that before the multimode fiber was defined as the coupling efficiency (η). The measured coupling efficiencies for both the e- and o-rays, represented by the optical-power attenuation (i.e., $10 \times \log_{10}(\eta)$) as a function of P_{LC}, are presented in Fig. 3(a). The corresponding optical-power attenuation as a function of the applied voltage V_2 is also plotted in Fig. 3(b); the relation between P_{LC} and the applied voltage is provided in Fig. 2(e). The minimum optical attenuation of the e-ray

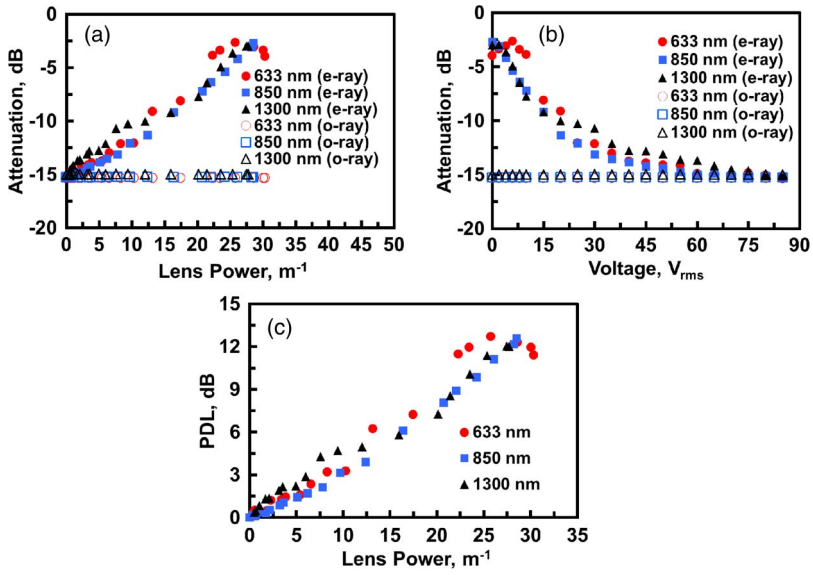

Fig. 3. (a) Optical-power attenuation as a function of (a) the lens power P_{LC} and (b) the applied voltage V_2 at various wavelengths for both e-rays and o-rays. (c) Polarization-dependent loss (PDL) as a function of lens power at various wavelengths.

was -2.65 dB, -2.70 dB, or -2.98 dB at wavelengths of 633 nm, 850 nm, and 1300 nm, respectively. Moreover, by varying P_{LC}, the attenuation of the e-ray could be controlled from its maximum value to ~ -15 dB, whereas the attenuation of the o-ray remained ~ -15 dB for all applied voltages. This result indicates that the LC lens behaved as a tunable linear polarizer because the transmission power of the e-ray was far larger than that of the o-ray. The extinction ratio (ER) is defined as the ratio of the transmittance of the e-ray to that of the o-ray, equal to $10 \times \log_{10}(T_{e-ray}/T_{o-ray})$, where T_{e-ray} and T_{o-ray} are the transmittances of the e-ray and o-ray, respectively. The ER is also referred to as the PDL [25], and then the data presented in Fig. 3(a) can therefore be converted to PDL as a function of P_{LC}, as shown in Fig. 3(c). In Fig. 3(c), the PDL decreases with decreasing P_{LC} because the focused beam size of the e-ray becomes larger as P_{LC} decreases, which enhances the optical attenuation of the e-ray. The maximum PDL values were found to be 12.7 dB at 633 nm, 12.6 dB at 850 nm, and 12.0 dB at 1300 nm. Although the attenuations and PDLs for the same P_{LC} are different at different wavelengths, it is still possible to adjust P_{LC} by varying the applied voltages to obtain the same attenuation and PDL at different wavelengths. Therefore, our electrically tunable polarizer can achieve a stable, wideband polarization selectivity. Fig. 3(a)–(c) indicate that an LC lens combined with a multimode fiber can serve as a variable polarizer for a wide range of wavelengths.

To further investigate the beam waist as a function of P_{LC}, we first estimated the beam waist using Eq. (5) with the experimental parameter $\rho = 50$ μm based on the assumption of an ideal Gaussian beam $(M^2 = 1)$. The results for the e-ray and o-ray are plotted in Fig. 4(a) and (b), respectively. When $P_{LC} = 0$, the beam waists for both e- and o-rays are approximately 400 μm, which is larger than the core radius $(\sim 50$ μm$)$. As a result, the optical attenuation is high $(\sim -15$ dB$)$, as shown in Fig. 3(a). The beam waist w for the e-ray decreases with increasing P_{LC}, leading to an increase in the coupling efficiency and a decrease in the optical attenuation. When P_{LC} reaches its maximum value, the smallest achievable beam waists for the e-ray are 80 μm at $\lambda = 633$ nm, 81 μm at $\lambda = 850$ nm, and 85 μm at $\lambda = 1300$ nm. The coupling efficiency reaches its maximum and the optical attenuation reaches its minimum simultaneously for these beam-waist values because the beam waists are as similar as possible to the core radius of the fiber $(\sim 50$ μm$)$. On the other hand, the beam waist of the o-ray remains ~ 400 μm for all lens powers, and the attenuation remains at approximately -15 dB. Hence, an electrically tunable LC lens can be operated as an electrically tunable polarization-selective device with variable optical attenuation by

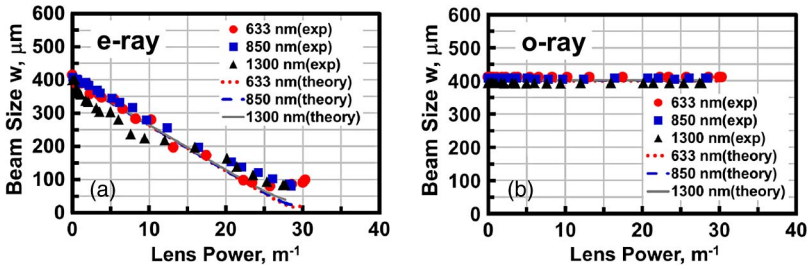

Fig. 4. Beam waist (w) as a function of lens power for (a) the e-ray and (b) the o-ray. The solid red dots, solid blue squares, and solid black triangles represent experimental results obtained at different wavelengths. The red dotted line, blue dashed line, and gray solid line represent the theoretical results calculated at different wavelengths.

manipulating the beam waist of the e-ray that couples to the fiber. We also calculated the beam waist w using Eq. (3), based on the assumption of an ideal thin lens. The calculated theoretical beam waists as a function of P_{LC} for $w_o = 0.4$ mm, $f_{\min} = 34.0$ and $d = 12.5$ cm at various wavelengths are presented in Fig. 4(a) and (b). In these figures, it is evident that the experimental results and theoretical results are in good agreement. In Fig. 4(a), the theoretical minimum beam waists of the e-ray are 17 μm at $\lambda = 633$ nm, 24 μm at $\lambda = 850$ nm, and 40 μm at $\lambda = 1300$ nm. The experimental minimum beam waists are somewhat larger than the theoretical ones because the phase profile of the LC lens is not a perfectly parabolic profile, and the thin-lens approximation is therefore not fully satisfied. The inhomogeneous LC materials may also produce some scattering, which would enlarge the beam waist. In addition, the experimental minimum beam waists are still larger than the core radius of the fiber ($\sim$50 μm). This is the reason why the minimum optical attenuation is only ~ -2.65 dB (shown in Fig. 3(a)). The minimum power attenuation that can be obtained using a traditional GRIN lens for coupling is $\sim$0.1 dB. To further reduce the minimum optical attenuation to achieve a large ER, the minimum beam waist must be further reduced, which can be achieved by using an LC lens with greater optical power and a large tunable range. In principle, a large electrically tunable range can be achieved by increasing the thickness of the LC layers or by using LC materials with high birefringence.

The response times of the LC lens were also measured. The measured response times were 382 ms and $\sim$762 ms when P_{LC} was switched between 30 m^{-1} and 0, respectively (the data are not shown here). The total response time can be further reduced to less than 100 ms using the overdriving method [1]. By adding polymer networks to nematic LC materials or blue-phase LCs, the response time can be reduced to the msec to sub-msec level [9], [26]. The insertion of a polymeric layer with a spatial distribution of permittivities into an LC lens can reduce the voltage below 10 V_{rms} [27]. Our LC lens could be combined with an LC device that exhibits anisotropic scattering properties, such as stretched polymer-dispersed LCs (PDLC), to enhance the PDL [28]. Moreover, the experimental results indicate that the transmittance (T) after passing through the LC lens at a wavelength of 1300 nm is approximately 8.7 dB ($T \sim 13.5\%$). This loss of transmittance predominantly originates from the loss in the ITO layer with a transmittance of 4.3 dB ($T \sim 37.2\%$), and the loss in the LC layer with a transmittance of 0.1 dB ($T \sim 97.7\%$). To increase the transmittance, other materials could be used for the conductive electrodes instead of ITO.

4. Conclusion

A broadband tunable polarizer based on an electrically tunable LC lens was demonstrated. By tuning P_{LC}, the beam size of the e-ray that couples into the fiber is changed, while the beam size of the o-ray remains the same. In addition, the PDL and optical-power attenuation of the e-ray also vary with P_{LC}. The experimental PDL was found to be greater than 12 dB in the visible and near-infrared spectral regions. In fiber systems with broad bandwidths, this LC lens is a promising candidate for use as a compact fiber polarizer. The primary advantage of this LC lens approach is the ability to integrate the functionalities of a GRIN lens, a polarization splitter, and an attenuator

into a fiber system using a single LC lens. The concept presented here can also be applied to other structures of LC lenses or other tunable anisotropic focusing optical components. Potential applications of this concept include chemical and biological optical sensors, fiber-optic gyroscopes and supercontinuum light polarizers.

References

[1] D. K. Yang and S. T. Wu, *Fundamentals of Liquid Crystal Devices*. Chichester, U.K.: Wiley, 2006.
[2] S. Sato, "Liquid-crystal lens-cells with variable focal length," *Jpn. J. Appl. Phys.*, vol. 18, no. 9, pp. 1679–1684, 1979.
[3] H. Ren and S. T. Wu, *Introduction to Adaptive Lenses*. Hoboken, NJ, USA: Wiley, 2012.
[4] H. C. Lin, M. S. Chen, and Y. H. Lin, "A review of electrically tunable focusing liquid crystal lenses," *Trans. Elect. Electron. Mater.*, vol. 12, no. 6, pp. 234–240, 2011.
[5] S. J. Woltman, G. P. Crawford, and G. D. Jay, *Liquid Crystals: Frontiers in Biomedical Applications*. Hackensack, NJ, USA: World Scientific, 2007.
[6] Y. H. Lin *et al.,* "A sperm testing device on a liquid crystal and polymer composite film," *J. Nanomedicine Nanotechnol.*, vol. S9, no. 001, pp. 1–5, 2011.
[7] Y. H. Lin *et al.,* "A biosensor of high-density lipoprotein of human serum on a liquid crystal and polymer composite film," in *Proc. Liquid Crystals XVII*, 2013, vol. 8828, p. 88280I.
[8] K. Hirabayashi, M. Wada, and C. Amano, "Optical-fiber variable-attenuator arrays using polymer-network liquid crystal," *IEEE Photon. Technol. Lett.*, vol. 13, no. 5, pp. 487–489, May 2001.
[9] Y. H. Wu *et al.,* "Variable optical attenuator with a polymer-stabilized dual-frequency liquid crystal," *Appl. Opt.*, vol. 44, no. 20, pp. 4394–4397, Jul. 2005.
[10] E. Brasselet, N. Murazawa, H. Misawa, and S. Juodkazis, "Optical vortices from liquid crystal droplets," *Phys. Rev. Lett.*, vol. 103, no. 10, p. 103903, 2009.
[11] B. Y. Wei *et al.,* "Generating switchable and reconfigurable optical vortices via photopatterning of liquid crystals," *Adv. Mater.*, vol. 26, no. 10, pp. 1590–1595, Mar. 2014.
[12] J. Feng *et al.,* "Fiber-optic pressure sensor based on tunable liquid crystal technology," *IEEE Photon. J.*, vol. 2, no. 3, pp. 292–298, Jun. 2010.
[13] Q. Bao *et al.,* "Broadband graphene polarizer," *Nature Photon.*, vol. 5, pp. 411–415, 2011.
[14] Y. Lin, J. Guo, and R. G. Lindquist, "Demonstration of an ultra-wideband optical fiber inline polarizer with metal nano-grid on the fiber tip," *Opt. Exp.*, vol. 17, no. 20, pp. 17849–17854, Sep. 2009.
[15] H. C. Lin and Y. H. Lin, "A fast response and large electrically tunable-focusing imaging system based on switching of two modes of a liquid crystal lens," *Appl. Phys. Lett.*, vol. 97, no. 6, pp. 063505-1–063505-3, Aug. 2010.
[16] H. C. Lin and Y. H. Lin, "An electrically tunable focusing liquid crystal lens with a built-in planar polymeric lens," *Appl. Phys. Lett.*, vol. 98, no. 8, pp. 083503-1–083503-3, Feb. 2011.
[17] H. C. Lin and Y. H. Lin, "An electrically tunable focusing pico-projector adopting a liquid crystal lens," *Jpn. J. Appl. Phys.*, vol. 49, no. 10, p. 102502, 2010.
[18] Y. H. Lin, M. S. Chen, and H. C. Lin, "An electrically tunable optical zoom system using two composite liquid crystal lenses with a large zoom ratio," *Opt. Exp.*, vol. 19, no. 5, pp. 4714–4721, Feb. 2011.
[19] Y. S. Tsou, Y. H. Lin, and A. C. Wei, "Concentrating photovoltaic system using a liquid crystal lens," *IEEE Photon. Technol. Lett.*, vol. 24, no. 24, pp. 2239–2242, Dec. 2012.
[20] H. C. Lin, N. Collings, M. S. Chen, and Y. H. Lin, "A holographic projection system with an electrically tuning and continuously adjustable optical zoom," *Opt. Exp.*, vol. 20, no. 25, pp. 27222–27229, Dec. 2012.
[21] H. S. Chen and Y. H. Lin, "An endoscopic system adopting a liquid crystal lens with an electrically tunable depth-of-field," *Opt. Exp.*, vol. 21, no. 15, pp. 18079–18088, Jul. 2013.
[22] Y. H. Lin and H. S. Chen, "Electrically tunable-focusing and polarizer-free liquid crystal lenses for ophthalmic applications," *Opt. Exp.*, vol. 21, no. 8, pp. 9428–9436, Apr. 2013.
[23] J. Niu and J. Xu, "Coupling efficiency of laser beam to multimode fiber," *Opt. Commun.*, vol. 274, no. 2, pp. 315–319, Jun. 2007.
[24] M. Ye, B. Wang, and S. Sato, "Liquid crystal lens with a focal length that is variable in a wide range," *Appl. Opt.*, vol. 43, no. 35, pp. 6407–6412, Dec. 2004.
[25] K. Zhou, G. Simpson, X. Chen, L. Zhang, and I. Bennion, "High extinction ratio in-fiber polarizers based on 45° tilted fiber Bragg gratings," *Opt. Lett.*, vol. 30, no. 11, pp. 1285–1287, Jun. 2005.
[26] Y. H. Lin *et al.,* "Polarizer-free and fast response microlens arrays using polymer-stabilized blue phase liquid crystals," *Appl. Phys. Lett.*, vol. 96, no. 11, pp. 113505-1–113505-3, Mar. 2010.
[27] H. C. Lin and Y. H. Lin, "An electrically tunable-focusing liquid crystal lens with a low voltage and simple electrodes," *Opt. Exp.*, vol. 20, no. 3, pp. 2045–2052, Jan. 2012.
[28] I. Amimori, J. N. Eakin, G. P. Crawford, N. V. Priezjev, and R. A. Pelcovits, "Optical and mechanical properties of stretched PDLC films for scattering polarizers," in *SID Int. Symp. Dig. Tech.*, vol. 33, no. 1, pp. 834–837, 2002.